Journal of Physics and Chemistry of Solids 119 (2018) 258–264

Contents lists available at ScienceDirect

Journal of Physics and Chemistry of Solids

journal homepage: www.elsevier.com/locate/jpcs

Design of a remote sprayed fast-curing γ-radiation-shielding material used in the collection of the leaked radioactive waste

Feida Chen[a,b], Minxuan Ni[a], Xiaobin Tang[a,b,*], Yun Zhang[a], Tuo Chen[a], Da Chen[a,b]

[a] Department of Nuclear Science & Engineering, Nanjing University of Aeronautics and Astronautics, Nanjing, 211100, China
[b] Jiangsu Key Laboratory of Nuclear Energy Equipment Materials Engineering, Nanjing, 211100, China

ARTICLE INFO

Keywords:
Gamma radiation-shielding material
Remote sprayed
Thermal stability
Mechanical properties

ABSTRACT

This work designed and measured a remote sprayed fast-curing γ-radiation-shielding material that is used to encapsulate and collect radioactive wastes from places far away from high radiation areas in case of radioactive waste leakage accidents. The influence of the chemical composition design on curing time, shielding performance, thermal stability and mechanical performance of the γ-radiation-shielding material is discussed. Results showed that with the addition of catalysts, the cream time of the γ-radiation-shielding material increased remarkably to allow it to be ejected, while the tack-free time of the solidified composite material decreased to guarantee good encapsulation of the radioactive wastes. Due to the denser microstructure, the γ-radiation-shielding material with bis(2-dimethylaminoethyl) ether and phosphorus flame retardant V-490 show better γ-radiation-shielding performance and mechanical properties than other products. When the shielding functional filler content reached 60%, the composite presented excellent comprehensive properties and a good application prospect.

1. Introduction

With the wide application of nuclear technology, especially with the rapid development of the nuclear power industry, radioactive waste leakage accidents and nuclear facility decommissioning present great challenges for us [1–3]. In these cases, substantial amounts of radioactive wastes need to be adsorbed, adhered and encapsulated to reduce pollution to the environment. In previous studies, portable lead bricks or flexible shielding materials, such as lead rubber and lead-free polymer composites, are generally utilized to cover and segregate wastes [4]. However, rescuers still have to get close enough to the radioactive wastes to complete the decontamination operation. To protect rescuers from radiation threat during the radioactive waste collection process, radiation shielding materials with distinctive technology route will be necessary.

In this study, we developed a remote sprayed fast-curing γ-radiation-shielding material based on polyurethane (PU). As shown in Fig. 1, it can be ejected far away from where radioactive wastes are located and encapsulate the wastes rapidly by forming a fully sealed layer so that rescuers can be protected from the threat of radiation exposure as much as possible. The active isocyanate in the PU system can react with the absorbed bound water on the surface of different materials to form firm hydrogen bonds, which will induce the PU materials to adhere to the radioactive wastes [5–7].

To optimize the properties of the γ-radiation-shielding material, making it more suitable for practical applications, the influence of the chemical composition design of the material is discussed. In this study, three different PU matrices were designed, and different contents of the filler were added to the matrix to optimize the curing time, microstructure, γ-radiation-shielding performance, flame-retardant performance, thermal stability and mechanical properties of the shielding materials.

2. Experimental methods

2.1. Materials

As shown in Fig. 1, the PU matrix designed in this work is composed of two parts. Component A consists of polyether polyols, surfactant, catalysts, blowing agent, and flame retardant, while component B contains isocyanate. Each part exists in a liquid state at room temperature, but solidifies immediately when mixed with others through the following action:

$$\mathrm{R{-}NCO + R1{-}OH = R{-}NHCOO{-}R1} \quad (1)$$

The products R—NHCOO—R1 are called PU and can be used to

* Corresponding author. Department of Nuclear Science & Engineering, Nanjing University of Aeronautics and Astronautics, Nanjing 211100, China.
E-mail address: tangxiaobin@nuaa.edu.cn (X. Tang).

https://doi.org/10.1016/j.jpcs.2018.04.013
Received 13 November 2017; Received in revised form 12 April 2018; Accepted 13 April 2018
Available online 16 April 2018
0022-3697/

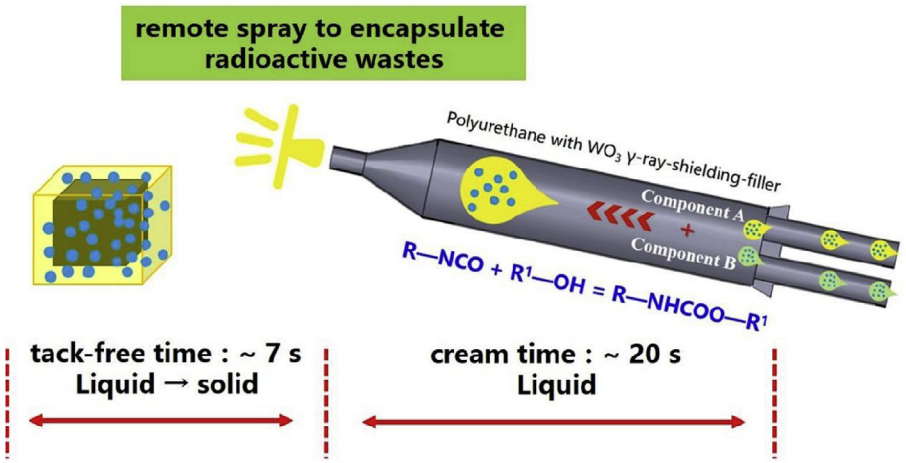

Fig. 1. Illustration of the design principle of fast-curing flame-retardant γ-ray-shielding composites for nuclear facility decommissioning.

Table 1
Detailed formula of the three different PU matrices.

Matrix component	System 1 content (wt%)	System 2 content (wt%)	System 3 content (wt%)
Polyether 4110	37.9	38.1	34.8
Polyether 204	9.5	9.5	8.7
V-490	–	–	8.7
Compound catalyst 1	1.4	–	–
Compound catalyst 2	–	1.4	1.3
Simethicone	0.9	0.9	0.9
Distilled water	0.5	–	–
PM-200	49.8	50.1	45.6

encapsulate the radioactive materials. In general, the two components of PU are fluidized and can solidify rapidly at room temperature. The feature fits the engineering application of remote spray well. In this work, three advanced PU matrix systems with ameliorative catalyst were designed and prepared to investigate radiation shielding performance. The detailed formulas of the three PU matrices are shown in Table 1. In the table, polyether 4110 (430–450 mg KOH/g, 2500–3000 mPa s) and polyether 204 (270–290 mg KOH/g, 60–80 mPa s) are polyether polyols, one of the two main ingredients of PU; the other is polymethylene diisocyanate (PMDI) PM200 (150–250 mPa s, NCO: 30.5%–32%). Catalyst 1 is a mixture of pentamethyl-diethylenetriamine, dibutyltin dilaurate, and distilled water. Catalyst 2 is a mixture of modified bis(2-dimethylaminoethyl) ether and dibutyltin dilaurate. V-490 is diethyl ethylphosphonate, which is used as a flame retardant. Simethicone is used as the surfactant.

Besides the matrix, the component of γ-radiation shielding functional fillers was also studied in the work. Compared with traditional lead materials, tungsten possesses several desirable properties. Aside from its stable chemical, physical, and excellent shielding properties, it does not have the toxicity of lead [8–10]. Therefore, WO_3 was selected as the shielding filler in this study. On the other hand, the smoke and gas generated in the burning process of PU pose great harm to human health [11,12]. The environment during nuclear facility decommissioning is complex and changeable. The composite flame-retardant property should thus be improved to suit the tough environment. Boride zinc (ZB) has a good synergistic flame-retardant effect compared with other flame retardants, and it can inhibit the generation of toxic smoke [13,14]. Therefore, ZB was selected as the flame retardant in this experiment.

Table 2 shows the proportion of the PU shielding composites. The fillers (WO_3 and ZB) were dried in a vacuum drying oven at 120 °C for 1 h and then cooled at room temperature. Fillers with the same weight were respectively added to components A and B (shown in Table 2).

Table 2
Proportion of PU shielding composites.

NO.	PU (wt%)	WO_3 (wt%)	ZB (wt%)
1	100	0	0
2	76	20	4
3	67	25	8
4	58	30	12
5	49	35	16
6	40	40	20

The components with fillers were mixed homogeneously and subsequently placed in an ultrasonic dispersing apparatus under 24 kHz for further dispersion for approximately 30 min. Finally, the two components with fillers were blended in a mixer at 2500 rpm for 5 s. The resulting reaction mixture was poured into a metal mold with a dimension of 10 × 10 × 5 cm^3.

2.2. Characterization

2.2.1. Curing time

The PU foam-curing process mainly involved two parameters about time. First, the time between the moment of mixing of components A and B and the moment the gas starts to generate and the solidification reaction begins is called as the cream time. Second, the time between the moment of mixing of components A and B and the moment the outer surface of the foam loses its stickiness as result of crosslinking completes is called as the tack-free time. Hence, the net curing time can be calculated by subtracting the cream time from the tack-free time. It represents the effective reaction velocity of the solidification reaction. In this study, the cream time and tack-free time were measured to characterize the curing process. The time parameters were recorded with a stopwatch.

2.2.2. Morphological observations

The micro-morphological features of the remote sprayed fast-curing shielding material were observed under a scanning electron microscope (SEM; JSM-7500, JEOL). The surfaces of the samples should be smooth and clean. First, the surfaces were sputter-coated with gold for observation. Then, the foam structure and distribution of the fillers were observed, and the diameter of the cell size was analyzed with a computer software to evaluate the performance of the composites.

2.2.3. γ-Radiation-shielding measurements

Under different irradiation point sources (^{238}Pu (43 keV, 99 keV, and 152 keV), ^{137}Cs (662 keV)), the shielding performances of the

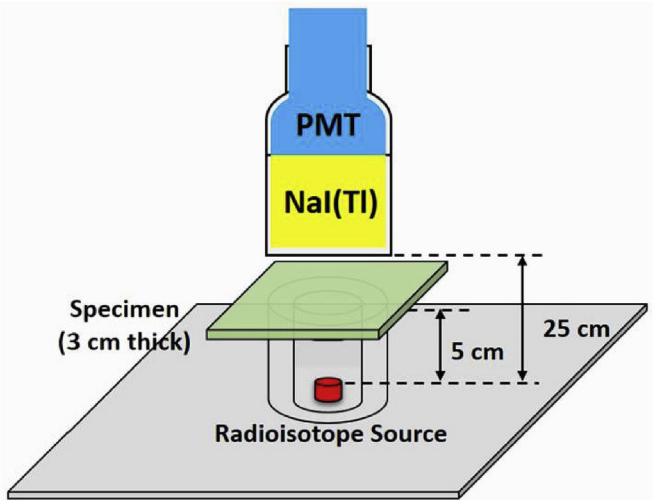

Fig. 2. Schematic diagram of the measure condition of the γ-ray shielding performance.

composite samples with different filler contents were measured with a NaI detector (ORTEC). As shown in Fig. 2, the distance between the top surface of the source and the samples was 5 cm. Meanwhile, the distance between the top surface of the source and the detector was 25 cm. The thickness of the samples was 3 cm.

2.2.4. Flame retardant test

The flame retardant properties of the shielding material were tested with an LOI apparatus. The test samples were created according to ASTM D 2863–97, and LOI was expressed as follows:

$$LOI = 100 \times [O_2] / ([O_2] + [N_2]) \quad (2)$$

2.2.5. Thermal stability test

Thermogravimetric (TG) analyses of shielding composites were conducted with the SDT-2960 TG analyzer. The tested samples (2 mg) were heated from 20 °C to 600 °C in a nitrogen atmosphere at a heating rate of 10 °C/min.

2.2.6. Compression performance test

The compression performance tests were performed according to ASTM D3410. The specimens used in the test were cut into 50 mm × 50 mm × 50 mm. In each batch, the number of specimens was more than 5. The compression loading rate was set to 5 mm/min. The compressive strength was calculated as follows:

$$\sigma_m = \frac{F_m}{A_0} \times 10^3, \quad (3)$$

where F_m is the maximum compression force when the relative deformation is less than 10% and A_0 is the cross-section area of the original specimens.

2.2.7. Surface adhesion performance test

Surface adhesion performance is very important for evaluating the encapsulation performance of the PU radiation shielding materials. In this study, the surface adhesion tests were performed according to ASTM D897–08. Before the test, the PU matrix materials were solidified between two T-type Q235 steel plates (shown in Fig. 3). The cross-section of the solidified PU matrix material is 2 cm × 2 cm and the thickness is 1.5 cm. The tensile tests were performed on the prepared specimens with a loading rate of 2 mm/min. The bonding strength was calculated as follows:

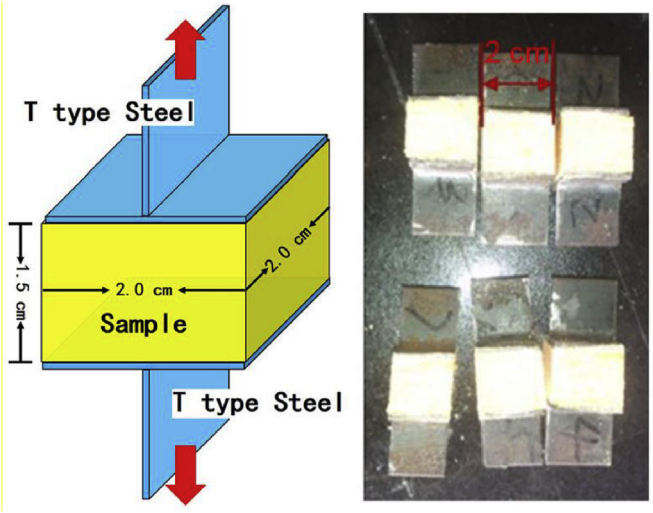

Fig. 3. Specimens of the surface adhesion performance test.

$$f_b = \frac{F}{A} \times 10^3 \quad (4)$$

where f_b is the tensile force and A is the cross-section area.

3. Results and discussion

3.1. Curing time

The cream time and tack-free time of the PU matrix radiation shielding materials with different catalytic systems were recorded to evaluate their curing property. The results are shown in Fig. 4.

As shown in Fig. 4, the cream time of system 1 was shorter than that of system 2 when the filler content is in the range of 0–60%. For system 2, the cream time was stable at about 20 s as the filler content increased, while the cream time of system 1 slightly dropped from 17 s to 12 s with the increase in filler content. The pentamethyl-diethylenetriamine in compound catalyst 1 could promote gas generation and shorten the cream time. Hence, system 2 with catalyst 2 had a longer reaction time. In our ideal design of the remote sprayed radiation-shielding materials, a longer cream time within a certain range means that we can eject from places farther away from the radioactive source. This provides better operability of the spray. On the other hand, the tack-free time of system 2 was shorter than that of system 1. The tack-

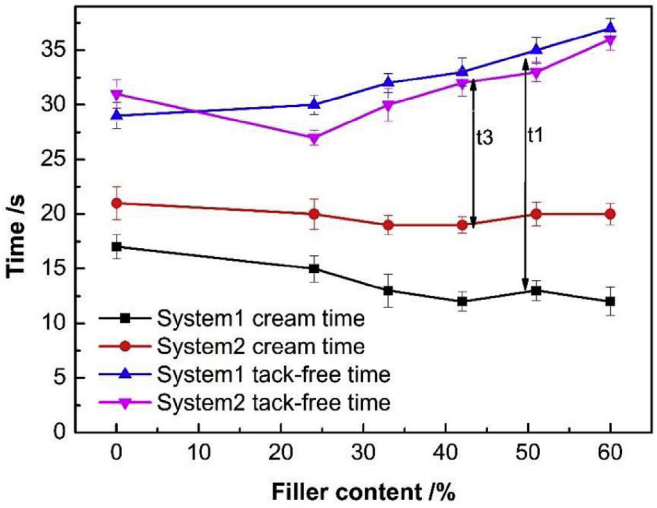

Fig. 4. Curing time of PU composites with different catalytic systems.

free time decreased at first and then increased with the increase in filler content. However, the addition of V-490 flame retardant had little effect on cream time and tack-free time. This phenomenon may be interpreted as follows: the modified bis ether(2-dimethylaminoethyl) in compound catalyst 2 was a gel catalyst, and it could promote the curing rate. In addition, as an amine catalyst, its activity might be improved by the alkaline WO_3. Consequently, the tack-free time decreased when the filler content was 20%. As the filler content increased, the filler blocked the reaction, and the tack-free time increased. The results show that system 2 had a long cream time and a short tack-free time. Although the tack-free time increased as the filler content increased, the net curing time t_3 remained smaller than t_1. The maximum value of t_3 was 16 s, and fast curing performance was still observed. Hence, system 2 is suitable for practical application.

3.2. γ-Radiation-shielding properties

The linear attenuation coefficient describes the fraction of a beam of X-rays or γ-rays that are absorbed or scattered per unit thickness of the absorber. If a sample is placed between a radioactive source with an intensity of I_0 and a detector, the intensity of beam I passing through the sample can be described as follows:

$$I = I_0 e^{-\mu x}, \quad (5)$$

where μ is the linear attenuation coefficient (cm^{-1}) and x is the thickness of the sample (cm). The higher the value of μ, the weaker the beam intensity that passes through the material and the better the shielding performance of the composite becomes.

In this study, the shielding performances of the composites were measured with a NaI detector and ^{238}Pu, ^{137}Cs radioactive source. The results are shown in Fig. 5. For all cases, the linear attenuation coefficient of the composite increased as the WO_3 filler content increased. When the filler content was the same, $\mu_{system3} > \mu_{system2} > \mu_{system1}$ for the same energy γ-ray shielding cases. In this work, the density was measured through the Archimedes densitometry. As shown in Table 3, the density of system 3 composites was the largest and system 2 was the second largest. Thus, it is not surprising that the three different systems with the same filler contents have different shielding properties. However, since the densities of the polymer matrix in the three systems were almost the same, it is surprising that the densities of the three systems differed so much.

Table 3
Density of different system composites with different filler contents.

No.	Filler content	System 1 density kg/m^3	System 2 density kg/m^3	System 3 density kg/m^3
1	0	88.6	215.35	298.5
2	24.6%	105.5	222.75	338.75
3	32.6%	134	261.8	394.5
4	41.8%	163	361.9	422
5	51.2%	202.7	421.55	533.75
6	60.4%	239	524.88	612

3.3. Morphological observations

The surfaces of the different system composites after cutting were investigated to observe the microstructure of foam and the dispersion quality of WO_3 and ZB filler particles. Fig. 6(a) and (b), and 6(c) show the micro-morphology of the three different PU matrices. Fig. 6(d) and (e) are the SEM micrographs of system 3 when the filler contents were 32.6% and 60.4%, respectively. Fig. 6(f) is the microstructure of sample 3–6 under 1000 magnification. Table 4 shows the average cell size of the samples corresponding to Fig. 6. As shown in Fig. 6(a)-(c), the cell sizes of systems 2 and 3 were smaller than that of system 1. The cell sizes of systems 2 and 3 presented an insignificant difference, but the average cell size of sample 3–1 was smaller than that of sample 2–1. The average cell size of system 3 decreased as the filler content increased in system 3. In general, the filler particles act as the bubble nucleation points. The addition of filler will promote the formation of bubble holes. However, the viscosity of the composites increases with the increase of filler content in the mean time. The diffusion behaviors of bubbles and the growth of bubble holes are inhibited by the sticky composites. Based on the competition results of the two effects, Fig. 6

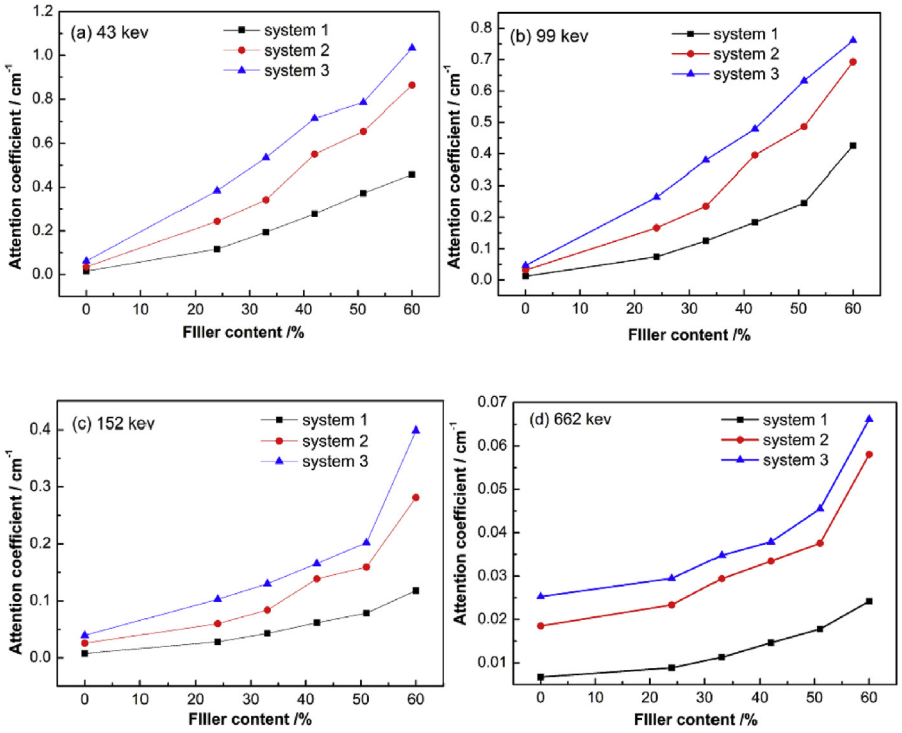

Fig. 5. Linear attenuation coefficient of the shielding materials in different systems at different γ-ray energies: (a) 43 keV, (b) 99 keV, (c) 152 keV, and (d) 662 keV.

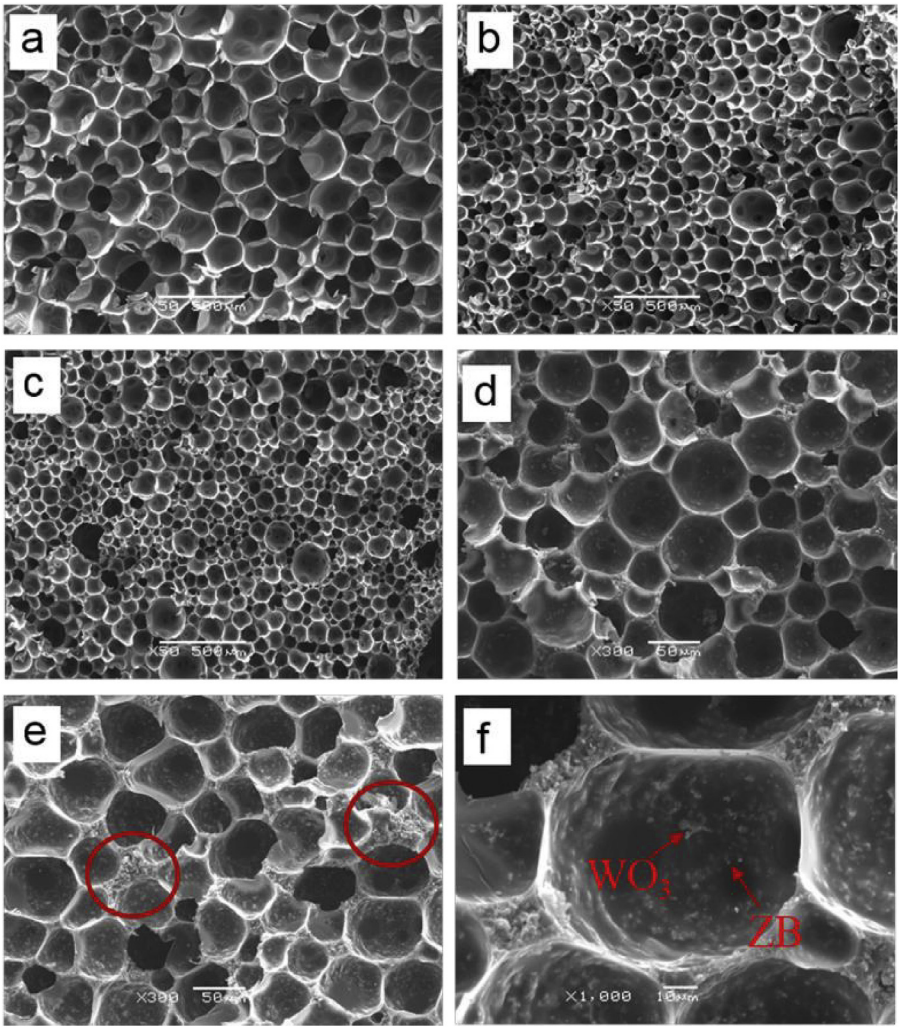

Fig. 6. Micro-morphology of different PU composites: (a) sample 1-1, (b) sample 2–1, (c) sample 3–1, (d) sample 3-3, (e) sample 3–6, and (f) microstructure of sample 3–6 (magnification: × 1000).

Table 4
Average cell size of different samples.

Sample No.	Average cell size (μm)
1–1	192.73
2–1	106.18
3–1	94.92
3–3	43.73
3–6	41.94

and Table 4 show that the PU composites became denser with the addition of fillers, because the growth of bubble holes was inhibited. However, when the filler content exceeded 33%, the average cell size of the composite exhibited a minimal change. The inhibition effect tends to be saturated. Many of the agglomerates (marked with circles) observed in Fig. 6(e) indicated that the matrix could no longer accommodate more fillers when the filler content reached 60%. In Fig. 6(f), the fillers mainly existed in the plateau borders, which were the intersections of the cell walls.

3.4. Flame retardant properties

Since the LOI of PU is approximately 17% (oxygen concentration in air is 21%), PU foam is too inflammable to be used in the nuclear industry. In addition, PU foam produces a large amount of harmful smoke during the combustion process. Improving the flame retardant of PU is important to protect workers in a complex decommissioning environment. Therefore, the ZB fillers were added to system 1, 2 and 3 composites, and V-490 together with ZB were added to system 3 for comparison in this study. The LOI of the shielding materials in the different systems was measured, and the results are shown in Table 5. The LOI of system 1 composite increased as the ZB filler content increased. The LOI of system 2 composite was larger than that of system 1 at the same filler content. This phenomenon mainly stemmed from the fact that ZB could produce a transparent material covering the sample surface during combustion, and this covering layer could isolate oxygen to binder burning. Combined with the results of the microstructure of systems 1 and 2 shown in Fig. 6, ZB gathered at the interfaces of the small cells in the PU matrix. In the case of smaller cell size, more interface area can

Table 5
LOI of the shielding materials in different systems.

No.	Filler content	System 1 LOI	System 2 LOI	System 3 LOI
1	0	16.5 ± 0.5	17.4 ± 0.4	21.5 ± 0.2
2	24.6%	16.9 ± 0.3	17.9 ± 0.2	22.2 ± 0.2
3	32.6%	17.3 ± 0.2	18.5 ± 0.2	22.9 ± 0.4
4	41.8%	18 ± 0.5	19.2 ± 0.3	23.6 ± 0.3
5	51.2%	18.6 ± 0.4	19.9 ± 0.2	24.4 ± 0.3
6	60.4%	19.5 ± 0.3	20.8 ± 0.3	25.8 ± 0.2

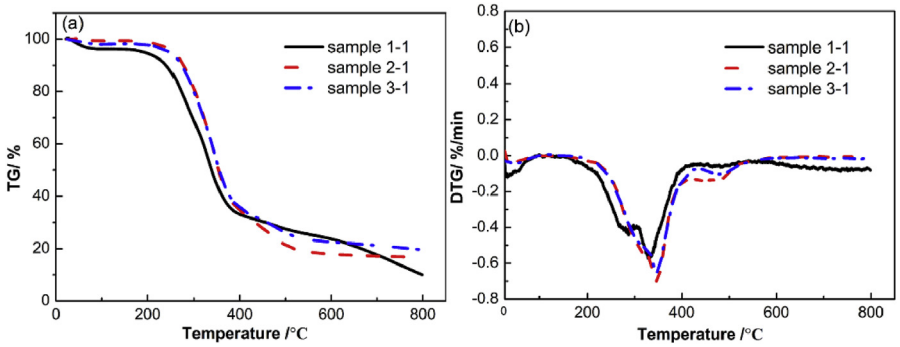

Fig. 7. TG and DTG curves of the three different system PU matrices.

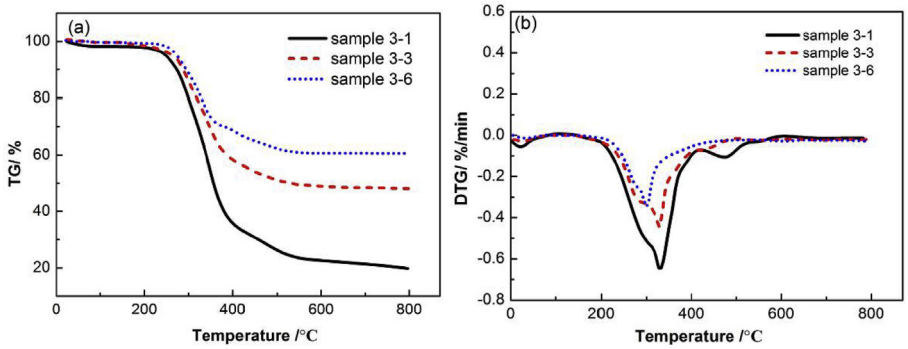

Fig. 8. TG and DTG curves of system 3 composite with different filler contents.

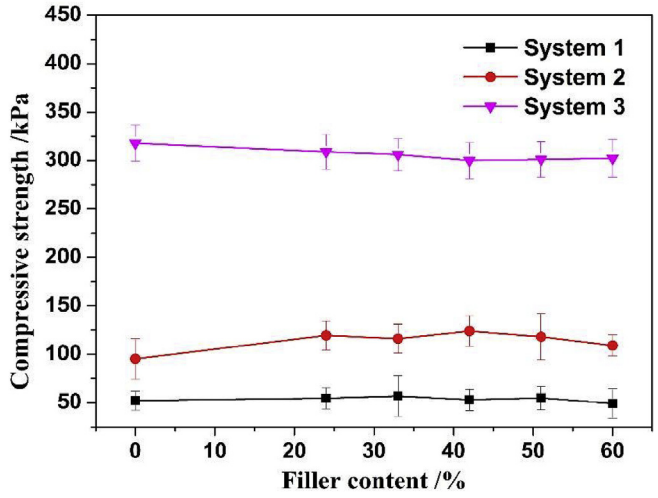

Fig. 9. The compressive strength of the three different system PU matrices.

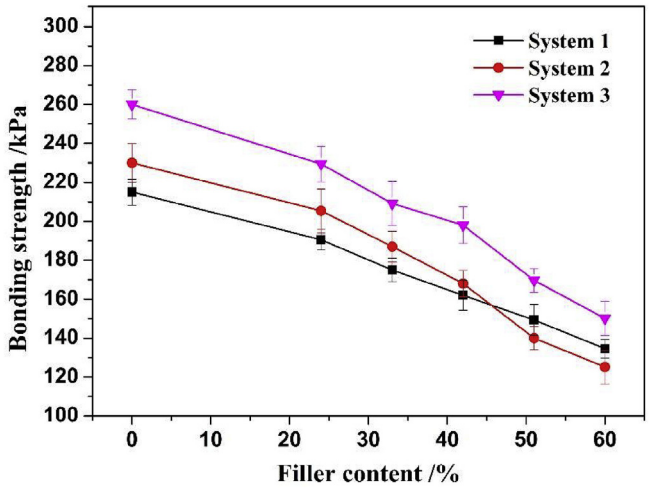

Fig. 10. The bonding strength of the three different system PU matrices.

be observed in system 2. Hence, the effect of ZB in inflaming retarding was more effective in system 2 than that in system 1. Moreover, after adding the phosphorus flame retardant V-490, the LOI of system 3 increased further. The LOI of system 3 PU matrix reached 21.5%. With the increase in filler content, the LOI growth rate of system 3 became larger than those of systems 1 and 2. It had the best flame-retardant property with an LOI of 25.8% when the filler content in system 3 was 60%. Since the oxygen concentration in air is 21%, the flame-retardant properties of this PU system have been improved significantly. During this process, the phosphorus flame retardant V-490 reacted with the combustible gas produced by the burning of PU. The consumption of the combustible matter is one of the important factors to prevent continued combustion.

3.5. Thermal stability

The radioactive source produces certain heat during the decay process. If radioactive waste needs to be sequestrated for a long time, excellent thermal stability is important to ensure radiation safety. Fig. 7 shows the typical TG and DTG curves of the three different system materials. For sample 1-1, the decomposition temperature was very low. It lost nearly 5% weight when the temperature reached 60 °C, then kept stable in the temperature range of 60–170 °C. Beyond 260 °C, the PU shielding material left only 90% weight. In contrast, samples 2–1 and 3–1 were stable below 200 °C. They disintegrated to their 90% weight until 310 °C. However, all three systems left only 40% weight when the temperature rose to 400 °C. The addition of V-490 exerted little effect on the thermal stability of PU radiation shielding materials. Fig. 7(b) shows the DTG curves of the three different system matrices. A

trend similar to that described above can be observed. When we compare the main components of system 1 and system 2, the catalyst added in system 1 had a substantial amount of small molecular substances. Because of the instability of the small molecular substances, system 1 begins to resolve even at low temperature. Hence, the thermal stabilities of PU radiation shielding materials improved after the catalyst which contains unstable small molecular substances was replaced.

Fig. 8 shows the TG and DTG curves of system 3 composite with different filler contents. The initial degradation temperature (T_i), cited as the characteristic temperature for assessing the thermal stability property, was also determined as the temperature at which 5% degradation occurred [15]. The T_i values for system 3 composites with filler contents of 0%, 32.6%, and 60.4% were measured to be 247 °C, 271 °C, and 279 °C, respectively. In Fig. 8(b), the degradation rate of system 3 composite decreased as the filler content increased. This result indicates that the thermal stability of the composite improved with the increase in filler content. Hence, system 3 composite had the best thermal stability at a filler content of 60%.

3.6. Compression performance

As shown in Fig. 9, the compression performance of system 1 was the worst among the three materials, and the compressive strength of system 3 was significantly higher than the other two. Since the catalyst in system 1 promotes gas generation during solidifying, the cell structure formed inside was large and the cell wall was thin, which explains why this system had the poorest compression performance. In system 2, the cell structure was relatively dense due to the optimized catalyst. Hence, the compressive strength increased. Furthermore, from the compression performance of system 3, we speculate that the flame retardant V-490 attended the solidifying reaction to form a more solid cell structure. The average cell sizes of the three system materials shown in Table 3 also indicate that the flame-retardant refined the cell structure. For all three systems, the compressive strength varied little with the increase of the filler content.

3.7. Surface adhesion performance

As described above, the active isocyanate group (-NCO) in the PU system can react with the absorbed bound water on the surface of different materials to form firm hydrogen bonds. This is the main source of the surface adhesion force of the PU materials. However, with the increase of filler content, the hydroxyl groups (-OH) contained in the surface of fillers consume more active isocyanate groups (-NCO) in the PU system. As shown in Fig. 10, the bonding strength of the PU material on the metal surface gradually decreased with the increase in the mass fraction of the functional filler. According to JC/T 998–2006, the bonding strength of rigid polyurethane foam that exceeds 100 kPa indicates that these materials can be considered good surface binders. Thus, the three different systems tested in the work are suitable for application in nuclear facility decommissioning.

4. Conclusion

Remote sprayed fast-curing γ-radiation-shielding composites based on PU were fabricated with WO_3 and ZB as filler materials. To optimize the curing time, flame retardant performance, thermal stability, shielding performance and mechanical properties of the composites, three different PU matrices were designed, and different contents of WO_3 and ZB fillers were added to the matrices. Results showed that with the addition of a suitable catalyst, the cream time of the two liquid components of the γ-radiation-shielding material increased remarkably to allow it to be ejected, while the tack-free time of the solidified composite material decreased to guarantee good encapsulation of the radioactive wastes. Meanwhile, the γ-radiation-shielding material was denser with the catalyst even at the same filler content so that the shielding performance and mechanical properties of the composite material were improved. The flame retardant V-490 also improved the flame-retardant performance and mechanical properties of the γ-radiation-shielding material. When the filler content reached 60%, the composite possessed excellent comprehensive properties and presented extensive potential applications for the protection of workers during radioactive waste leakage accidents and nuclear facility decommissioning.

Acknowledgment

Feida Chen and Minxuan Ni contributed equally to this work. This work was supported by the project supported by the Funding of Graduate Innovation Center in NUAA under Grant No. kfjj20150608 and Grant No. kfjj20160604, and the project funded by the Priority Academic Program Development of Jiangsu Higher Education Institutions (PAPD).

References

[1] V. Gil-Cerezo, E. Dominguez-Vilches, A. Gonzalez-Barrios, Current significant challenges in the decommissioning and environmental remediation of radioactive facilities: a perspective from outside the nuclear industry, J. Environ. Radioact. 171 (2017) 200–211.
[2] N. Shruti, Y. John, Polymer-composite materials for radiation protection, ACS Appl. Mater. Interfaces 4 (2012) 5717–5726.
[3] R. Periznez, S. Kyung-Suk, M. Byung, The behavior of ^{137}Cs in the North Atlantic Ocean assessed from numerical modeling: releases from nuclear fuel reprocessing factories, redissolution from contaminated sediments and leakage from dumped nuclear wastes, Mar. Pollut. Bull. 113 (2016) 343–361.
[4] H. Chai, X.B. Tang, M.X. Ni, F.D. Chen, Y. Zhang, D. Chen, Y.L. Qiu, Preparation and properties of novel, flexible, lead-free X-ray-shielding materials containing tungsten and bismuth (III) oxide, J. Appl. Polym. Sci. 133 (2016) 43012.
[5] G.A. Bockorny, M.M.C. Forte, S. Stamboroski, M. Noeske, A. Keil, W.L. Cavalcanti, Modifying a thermoplastic polyurethane for improving the bonding performance in an adhesive technical process, Appl. Adhe. Sci. 4 (2016) 1.
[6] H.B. Chen, Y.Y. Ao, D. Liu, H.T. Song, P. Shen, Novel neutron shielding alginate based aerogel with extremely low flammability, Ind. Eng. Chem. Res. 56 (2017) 8563–8567.
[7] H. Singh, Rigid polyurethane foam: a versatile energy efficient material, Key Eng. Mater. 678 (2016) 88–98.
[8] H. Turkez, B. Cakmak, K. Celik, Evaluation of the potential in vivo genotoxicity of tungsten (VI) oxide nanopowder for human health, Key Eng. Mater. 543 (2012) 89–92.
[9] J. Kim, D. Seo, B.C. Lee, Y.S. Seo, W.H. Miller, Nano-W dispersed gamma radiation shielding materials, Adv. Eng. Mater. 16 (2014) 1083–1089.
[10] J.H. Liu, Q.P. Zhang, N. Sun, Y. Zhao, R. Shi, Y.L. Zhou, J. Zheng, Elevated gamma-rays shielding property in lead-free bismuth tungstate by nanofabricating structures, J. Phys. Chem. Solid. 112 (2018) 185–189.
[11] W. Xi, L.J. Qian, Z.G. Huang, Y.F. Cao, L.J. Li, Continuous flame-retardant actions of two phosphate esters with expandable graphite in rigid polyurethane foams, Polym. Degrad. Stabil. 130 (2016) 97–102.
[12] Q. Wu, Q. Zhang, L. Zhao, S.N. Li, L.B. Wu, J.X. Jiang, L.C. Tang, A novel and facile strategy for highly flame retardant polymer foam composite materials: transforming silicone resin coating into silica self-extinguishing layer, J. Hazard Mater. 336 (2017) 222–231.
[13] S.L. Li, B.H. Long, Z.C. Wang, Y.M. Tian, Y.H. Zheng, Q. Zhang, Synthesis of hydrophobic zinc borate nanoflakes and its effect on flame retardant properties of polyethylene, J. Solid State Chem. 183 (2010) 957–962.
[14] R. Jeencham, N. Suppakarn, K. Jarukumjorn, Effect of flame retardants on flame retardant, mechanical, and thermal properties of sisal fiber/polypropylene composites, Compos. B Eng. 56 (2014) 249–253.
[15] A.J. Gu, G.Z. Liang, Thermal degradation behavior and kinetic analysis of epoxy/montmorillonite nanocomposites, Polym. Degrad. Stabil. 80 (2003) 383–391.